



杭州电子科技大学  
Hangzhou Dianzi University

# Quantum Transport

DIRAC FERMION DISCUSSION GROUP

**Axia**

[xiamyphys@gmail.com](mailto:xiamyphys@gmail.com)





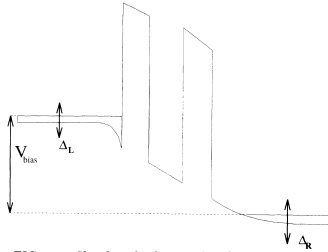


FIG. 1. Sketch of charge distribution in a three dimensional resonant-tunneling device under dc bias  $V_{\text{bias}} = \mu_L - \mu_R$  with a time modulation of amplitude  $\Delta_{L/R}$  superposed on the leads. As argued in the text, only a tiny fraction of charge carriers participates in setting up the voltage drop across the structure.

charge is quite strong, and hence the bias across a tunneling structure is caused by a relatively small excess of charge in accumulation and depletion layers. The formation of these layers then causes a rigid shift [see Eq. (2) below] of the bottom of the conduction band deeper in the leads, which is the origin of the rigid shift of energy levels in our treatment of a time-dependent bias.

The second frequency limit on our approach is that the buildup of electrons required for the formation of the accumulation and depletion layers must not significantly disrupt the coherent transport of electrons incident from the leads. One way to quantify this is to ask—what is the probability that an electron incident from the leads participates in the buildup of charge associated with a time-dependent bias? This probability will be the ratio of the net current density flowing into the accumulation region to the total incident flux of electrons. For a three-dimensional double-barrier resonant-tunneling structure (see Fig. 1) the ac charging the accumulation layer is  $I_{\text{acc}}^{\text{rms}} = 2\pi\nu CV^{\text{rms}}/A$ , where  $\nu$  is the driving frequency,  $C$  is the capacitance,  $V^{\text{rms}}$  is the applied bias, and  $A$  is the area. In comparison, the total incident flux is  $I_{\text{inc}} = 3/8 env_F$ . Using the parameters appropriate for a typical experiment (we use that of Brown *et al.*<sup>24</sup>), we find that up to 10 THz the probability of an electron participating in the charge buildup is only 1%. Summarizing, these estimates indicate that our approach should be accurate up to frequencies of tens of THz, which are large by present experimental standards, and consequently the analysis presented in what follows should be valid for most experimental situations.

### III. THEORETICAL TOOLS AND THE MODEL

#### A. Baym-Kadanoff-Keldysh nonequilibrium techniques

Here we wish to outline the physical background behind the Keldysh formulation, and in particular its con-

nection to tunneling physics. Readers interested in technical details should consult any of the many available review articles, such as Refs. 25–27. The basic difference between construction of equilibrium and nonequilibrium perturbation schemes is that in nonequilibrium one cannot assume that the system returns to its ground state (or a thermodynamic equilibrium state at finite temperatures) as  $t \rightarrow +\infty$ . Irreversible effects break the symmetry between  $t = -\infty$  and  $t = +\infty$ , and this symmetry is heavily exploited in the derivation of the equilibrium perturbation expansion. In nonequilibrium situations one can circumvent this problem by allowing the system to evolve from  $-\infty$  to the moment of interest (for definiteness, let us call this instant  $t_0$ ), and then continue the time evolution from  $t = t_0$  back to  $t = -\infty$ <sup>28</sup> (When dealing with quantities that depend on two time variables, such as Green functions, the time evolution must be continued to the later time.) The advantage of this procedure is that all expectation values are defined with respect to a well defined state, i.e., the state in which the system was prepared in the remote past. The price is that one must treat the two time branches on an equal footing (See Fig. 2).

A typical object of interest would be a two time Green function (see Appendix A); the two times can be located on either of the two branches of the complex time path (e.g.,  $\tau$  and  $\tau'$  in Fig. 2). One is thus led to consider  $2 \times 2$  Green-function matrices, and the various terms in the perturbation theory can be evaluated by matrix multiplication. Since the internal time integrations run over the complex time path, a method of bookkeeping for the time labels is required, and there are various ways of doing this. In the present work we employ a version of the Keldysh technique.

In the context of tunneling problems the time-independent Keldysh formalism works as follows. In the remote past the contacts (i.e., the left and right lead) and the central region are decoupled, and each region is in thermal equilibrium. The equilibrium distribution functions for the three regions are characterized by their respective chemical potentials; these do not have to coincide nor are the differences between the chemical potentials necessarily small. The couplings between the different regions are then established and treated as perturbations via the standard techniques of perturbation theory, albeit on the two-branch time contour. It is important to notice that the couplings do not have to be small, e.g., with respect level spacings or  $k_B T$ , and typically must be treated to all orders.

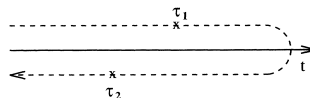


FIG. 2. The complex-time contour on which nonequilibrium-Green-function theory is constructed. In the contour sense, the time  $\tau_1$  is earlier than  $\tau_2$  even though its real-time projection appears larger.

The time-dependent case can be treated similarly. Before the couplings between the various regions are turned on, the single-particle energies acquire rigid time-dependent shifts, which, in the case of the noninteracting contacts, translate into extra phase factors for the propagators (but not in changes in occupations). The perturbation theory with respect to the couplings has the same diagrammatic structure as in the stationary case. The calculations, of course, become more complicated because of the broken time-translational invariance.

### B. Model Hamiltonian

We split the total Hamiltonian in three pieces:  $H = H_c + H_T + H_{cen}$ , where  $H_c$  describes the contacts,  $H_T$  is the tunneling coupling between contacts and the interacting region, and  $H_{cen}$  models the interacting central region, respectively. Below we discuss each of these terms.

#### 1. Contacts, $H_c$

Guided by the typical experimental geometry in which the leads rapidly broaden into metallic contacts, we view electrons in the leads as noninteracting except for an overall self-consistent potential. Physically, applying a time-dependent bias between the source and drain contacts corresponds to accumulating or depleting charge to form a dipole around the central region. The resulting electrostatic-potential difference means that the single-particle energies become time dependent:  $\epsilon_{k\alpha}^0 \rightarrow \epsilon_{k\alpha}^0(t) = \epsilon_{k\alpha}^0 + \Delta_\alpha(t)$  [here  $\alpha$  labels the channel in the left ( $L$ ) or right ( $R$ ) lead]. The occupation of each state  $k\alpha$ , however, remains unchanged. The occupation, for each contact, is determined by an equilibrium distribution function established in the distant past, before the time-dependence or tunneling matrix elements are turned on. Thus, the contact Hamiltonian is

$$H_c = \sum_{k,\alpha \in L,R} \epsilon_{k\alpha}(t) c_{k\alpha}^\dagger c_{k\alpha}, \quad (1)$$

and the exact time-dependent Green functions in the lead of the uncoupled system are

$$\begin{aligned} g_{k\alpha}^<(t, t') &\equiv i \langle c_{k\alpha}^\dagger(t') c_{k\alpha}(t) \rangle \\ &= i f(\epsilon_{k\alpha}^0) \exp \left[ -i \int_{t'}^t dt_1 \epsilon_{k\alpha}(t_1) \right] \\ g_{k\alpha}^{r,\alpha}(t, t') &\equiv \mp i \theta(\pm t \mp t') \langle \{ c_{k\alpha}(t), c_{k\alpha}^\dagger(t') \} \rangle \\ &= \mp i \theta(\pm t \mp t') \exp \left[ -i \int_{t'}^t dt_1 \epsilon_{k\alpha}(t_1) \right]. \end{aligned} \quad (2)$$

One should note that our model for  $g^<$  differs from the choice made in the recent study of Chen and Ting.<sup>15</sup> The difference does not affect calculations carried out to linear response in the ac drive, but is significant in nonlinear response. Specifically, Chen and Ting allow the electrochemical potential in the distribution function  $f$  to vary with time:  $\mu_L - \mu_R = e[V + U(t)]$ , where  $U(t)$  is the ac

signal. This assumption implies that the *total number* of electrons in the contacts varies with time. This behavior is inconsistent with what happens in real devices: it is only the relatively small number of electrons in the accumulation-depletion layers that is time dependent. In addition to the unphysical charge pileup in the contacts, the model of Chen and Ting leads to an instantaneous loss of phase coherence in the contacts, and hence does not display any of the interesting interference phenomena predicted by our phase-conserving model.

#### 2. Coupling between leads and central region, $H_T$

The coupling between the leads and the central (interacting) region can be modified with time dependent gate voltages, as is the case in single-electron pumps. The precise functional form of the time dependence is determined by the detailed geometry and by the self-consistent response of charge in the contacts to external driving. We assume that these parameters are known, and simply write

$$H_T = \sum_{\alpha, \alpha' \in L,R} [V_{\alpha\alpha'}(t) c_{\alpha'}^\dagger d_n + \text{H.c.}]. \quad (3)$$

Here  $\{d_n^\dagger\}$  and  $\{d_n\}$  form a complete orthonormal set of single-electron creation and annihilation operators in the interacting region.

#### 3. The central-region Hamiltonian $H_{cen}$

The form chosen for  $H_{cen}$  in the central interacting region depends on geometry and on the physical behavior being investigated. Our results relating the current to local properties, such as densities of states and Green functions, are valid generally. To make the results more concrete, we will discuss two particular examples in detail. In the first, the central region is taken to consist of noninteracting, but time-dependent levels,

$$H_{cen} = \sum_m \epsilon_m(t) d_m^\dagger d_m. \quad (4)$$

Here  $d_m^\dagger$  ( $d_m$ ) creates (destroys) an electron in state  $m$ . The choice (4) represents a simple model for time-dependent resonant tunneling. Below we shall present general results for an arbitrary number of levels, and analyze the case of a single level in detail. The latter is interesting both as an exactly solvable example, and for predictions of coherence effects in time-dependent experiments.

The second example we will discuss is resonant tunneling with electron-phonon interaction,

$$H_{cen}^{el-ph} = \epsilon_0 d^\dagger d + d^\dagger d \sum_{\mathbf{q}} M_{\mathbf{q}} [a_{\mathbf{q}}^\dagger + a_{-\mathbf{q}}]. \quad (5)$$

In the above, the first term represents a single site, while the second term represents the interaction of an electron on the site with phonons:  $a_{\mathbf{q}}^\dagger$  ( $a_{\mathbf{q}}$ ) creates (destroys) a phonon in mode  $\mathbf{q}$ , and  $M_{\mathbf{q}}$  is the interaction matrix element. The full Hamiltonian of the system





杭州电子科技大学  
Hangzhou Dianzi University

## AQM & SPD

**Axia**

[xiamyphys@gmail.com](mailto:xiamyphys@gmail.com)





## Rotations and Angular Momenta



Mengnan Chen (HDU)

Advanced Quantum Mechanics

November 8, 2023

3 / 66

## Finite Versus Infinitesimal Rotations

Consider a vector

$$\mathbf{v} = (V_x \ V_y \ V_z)^T,$$

after a rotation

$$\begin{pmatrix} V'_x \\ V'_y \\ V'_z \end{pmatrix} = R \begin{pmatrix} V_x \\ V_y \\ V_z \end{pmatrix}$$

with

$$R^T R = R R^T = 1,$$

leading to a property

$$\mathbf{v}^T \mathbf{v} = \mathbf{v}^T R^T R \mathbf{v},$$
$$V_x'^2 + V_y'^2 + V_z'^2 = V_x^2 + V_y^2 + V_z^2.$$



Mengnan Chen (HDU)

Advanced Quantum Mechanics

November 8, 2023

4 / 66



Likewise, we have

$$R_x(\epsilon) = \begin{pmatrix} 1 & 0 & 0 \\ 0 & 1 - \frac{\epsilon^2}{2} & -\epsilon \\ 0 & \epsilon & 1 - \frac{\epsilon^2}{2} \end{pmatrix},$$

and

$$R_y(\epsilon) = \begin{pmatrix} 1 - \frac{\epsilon^2}{2} & 0 & \epsilon \\ 0 & 1 & 0 \\ -\epsilon & 0 & 1 - \frac{\epsilon^2}{2} \end{pmatrix}.$$

◀ ▶ ⏪ ⏩ 🔍 🔄

Elementary matrix manipulations lead to

$$R_x R_y = \begin{pmatrix} 1 - \frac{\epsilon^2}{2} & 0 & \epsilon \\ \epsilon^2 & 1 - \frac{\epsilon^2}{2} & -\epsilon \\ -\epsilon & \epsilon & 1 - \epsilon^2 \end{pmatrix}$$

$$R_y R_x = \begin{pmatrix} 1 - \frac{\epsilon^2}{2} & \epsilon^2 & \epsilon \\ 0 & 1 - \frac{\epsilon^2}{2} & -\epsilon \\ -\epsilon & \epsilon & 1 - \epsilon^2 \end{pmatrix}$$

$$R_x R_y - R_y R_x = \begin{pmatrix} 0 & -\epsilon^2 & 0 \\ \epsilon^2 & 0 & 0 \\ 0 & 0 & 0 \end{pmatrix} = R_z(\epsilon^2) - 1,$$

where all terms of order higher than  $\epsilon^2$  have been ignored.

◀ ▶ ⏪ ⏩ 🔍 🔄

## Infinitesimal Rotations in Quantum Mechanics

Given a rotation operation characterized by an orthogonal  $3 \times 3$  matrix  $R$ , associate an operator  $\mathcal{D}(R)$  in the appropriate ket space such that

$$|\alpha\rangle_R = \mathcal{D}(R)|\alpha\rangle.$$

- For describing a spin-1/2, system with no other degrees of freedom,  $\mathcal{D}(R)$  is a  $2 \times 2$  matrix;
- for a spin-1 system,  $\mathcal{D}(R)$  is a  $3 \times 3$  matrix.

The appropriate infinitesimal operators could be written as

$$\hat{U}(\epsilon) = 1 - i\hat{G}\epsilon, \quad \hat{G}: \text{Hermitian}$$

We therefore define the angular-momentum operator  $\hat{J}_k$  for an infinitesimal rotation around the  $k$ th axis by angle  $d\phi$  can be obtained by letting

$$\hat{G} \rightarrow \frac{\hat{J}_k}{\hbar}, \quad \epsilon \rightarrow d\phi$$

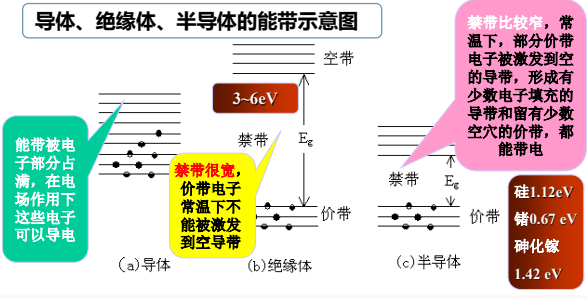
◀ ▶ ⏪ ⏩ 🔍 🔄





### 固体材料的分类（微观）——能带结构

#### 导体、绝缘体、半导体的能带示意图



### 半导体的种类及特性

#### 半导体的种类

- 元素半导体和化合物半导体
- 晶态半导体、非晶及多晶半导体
- 无机半导体和有机半导体
- 本征半导体和杂质半导体

#### 主要的元素和化合物半导体

元素半导体	IV族化合物半导体	III-V族化合物半导体	II-VI族化合物半导体
Si	SiC	AlP	ZnS
Ge	SiGe	AlAs	ZnSe
		AlSb	ZnTe
		GaP	CdS
		GaAs	CdSe
		GaSb	CdTe
		InP	
		InAs	
		InSb	

#### 半导体的基本特性

- 温度效应-----负温度系数
- 掺杂效应-----杂质敏感性
- 光电效应-----光电导
- 电场、磁场效应

### 固体（半导体）材料的分类——原子空间排列

- 单晶：原子排列长程有序，内部结构有周期性（长程有序：um量级），例如：单晶硅
- 非晶：原子排列无序，例如：玻璃（无序SiO<sub>2</sub>）
- 多晶：原子排列短程有序，由不同取向的单晶颗粒组成，例如：多晶硅



(a) Crystalline

单晶：周期性

25.0%

硅太阳能电池效率(实验室)



(b) Amorphous

非晶：无周期性

10.1%



(c) Polycrystalline

多晶：小区域周期性

20.4%

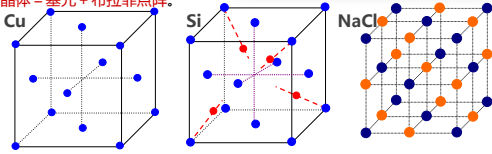


### 晶体结构的基本概念\*

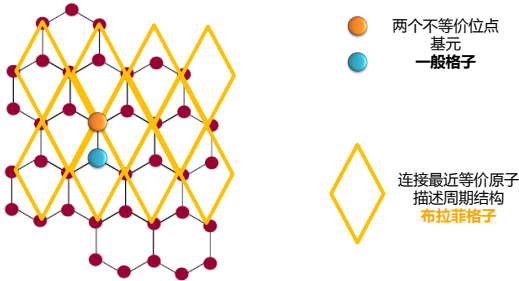
晶体结构 = 结构基元 + 点阵

- 基元：组成晶体的最小单元。
- 布拉非格子（点阵）
  - (1) 晶体一定具有平移周期性
  - (2) 每个格点周围环境完全相同
- 晶体 = 基元 + 布拉非点阵。

例如：Cu的面心立方晶格，Si的金刚石晶格和NaCl晶格**布拉非格子都是面心立方格子**，每个格点的基元分别为一个Cu、两个Si和一对Na<sup>+</sup>、Cl<sup>-</sup>离子。



### 一般格子和布拉非格子



原胞与晶胞的区别与联系

原胞	晶胞
晶格中 <b>体积最小</b> 的周期单元	体积较大的周期单元
每个原胞中实际上只包含一个格点。 每个原胞有 <b>8个顶角</b> ，每个顶角为相邻 <b>8个原胞</b> 所共有，所以， 每个原胞所含格点数为 <b><math>8 \times 1/8 = 1</math></b>	每个晶胞中所含格点数因结构而异。例： <b>面心立方晶格晶胞结构——立方体</b> ， <b>面心格点</b> ：两个相邻晶胞共有，只有 <b>1/2</b> 属于一个晶胞； <b>顶角格点</b> ：只有 <b>1/8</b> 属于一个晶胞； <b>总格点数</b> = <b><math>8 \times 1/8 + 6 \times 1/2 = 4</math></b>
原胞的体积可表示为： $v = \vec{a}_1 \cdot (\vec{a}_2 \times \vec{a}_3)$ <b>面心立方晶格的原胞体积</b> = <b><math>a^3/4</math></b>	晶胞体积是原胞体积的 <i>n</i> 倍 ( <i>n</i> 是该结构每个晶胞所含格点数) <b>面心立方结构晶胞体积</b> = <b><math>a^3</math></b>

### 小结:三种原胞特点

固体物理学原胞    结晶学原胞    维格纳-赛兹原胞

是**体积最小**的原胞，格点只在**顶角**上，每个原胞平均只含**一个格点**，其基矢常用  $\vec{a}_1, \vec{a}_2, \vec{a}_3$  来表示；

为同时反映晶体的**微观周期结构**和**晶体对称性**，通常选取**体积较大**的原胞，常称为“**晶胞**”，其格点**不只在顶角上**，还可分布在**体心和面心**处，每个原胞平均不只含一个格点，其基矢常用  $\vec{a}, \vec{b}, \vec{c}$  来表示；

是以一格点为中心，画中心到最近邻格点的**连线的垂直平分面**，围成的多面体称**维格纳-赛兹原胞**。它也是**体积最小**的原胞，其格点只在**中心**，每个原胞平均只含**一个格点**；











